

SUPPORTING INFORMATION

Design and synthesis of VO₂/MWCNT/GONR nanocomposites for ultrahigh-rate and long-life aqueous Zn-ion batteries

*Tzu-Ho Wu,^{*a} Cao-Feng Chen,^a Liang-Jun Guo,^a Chia-Liang Sun,^{*b,c} Tzu-Kuan Li,^a Kung-Yi Ni,^a Chen-Wei Tai,^d Chi-Chang Hu^d*

^a Department of Chemical and Materials Engineering, National Yunlin University of Science and Technology, Yunlin 64002, Taiwan. E-mail: wutzu@yuntech.edu.tw

^b Department of Chemical and Materials Engineering, Chang Gung University, Taoyuan 333323, Taiwan. E-mail: clsun@mail.cgu.edu.tw

^c Department of Neurosurgery, Linkou Chang Gung Memorial Hospital, Taoyuan 333423 Taiwan

^d Department of Chemical Engineering, National Tsing Hua University, 300044 Hsin-Chu, Taiwan.

1. Experimental Procedures

Chemicals.

Vanadyl (IV) acetylacetonate ($\text{VO}(\text{acac})_2$, 99%), L-Cysteine ($\text{C}_3\text{H}_7\text{NO}_2\text{S}$, 98%), ethanol (95%), and zinc di[bis(trifluoromethylsulfonyl)imide] ($\text{Zn}(\text{TFSI})_2$, 98%) were purchased from Acros Organics, Thermo Fisher Scientific, Taiwan Sugar Corporation, and Tokyo Chemical Industry, respectively. Potassium sulfate (K_2SO_4 , 99%) and N-methyl-2-pyrrolidone (NMP, 99%) were purchased from Sigma-Aldrich. MWCNTs were used as received from CNT Co., Ltd. (product name, CTube-120; diameter = 10–40 nm; length = 1–25 μm). H_2SO_4 , H_3PO_4 , and KMnO_4 were purchased from J.T. Baker. Zinc foil (99.98%, thickness = 0.25 mm), Super P (99%), and poly(vinylidene difluoride) (PVDF, 99%) were purchased from Alfa Aesar. The chemicals were used as received. CR2032 Coin-type cells, carbon paper substrates (GDS180S, thickness = 0.18 mm), glass fiber separator (GF6) were purchased from JuChen, CeTech, and Whatman, respectively.

Synthesis of $\text{VO}_2(\text{P})$.

The synthetic procedures for obtaining the $\text{VO}_2(\text{P})$ sample were adopted from a previous report.¹ Typically, $\text{VO}(\text{acac})_2$ (6 mmol), $\text{C}_3\text{H}_7\text{NO}_2\text{S}$ (48 mmol), and K_2SO_4 (1.67 mmol) were successively dissolved in 200 mL deionized water under magnetic stirring. Then, the precursor solution was transferred to a Teflon-lined stainless autoclave for the hydrothermal reaction at 180 °C for 24 h at a heating rate of 2 °C min^{-1} . After natural cooling, the resulting precipitate was thoroughly washed with deionized water and ethanol. After drying at 60 °C and grinding using a mortar, the powder product was put into a porcelain boat and heated to 120 °C for 6 h at a heating rate of 2 °C min^{-1} in air. The black $\text{VO}_2(\text{P})$ powder sample was collected after natural cooling.

Synthesis of MWCNT/GONR.

Multiwalled carbon nanotube/graphene nanoribbon (MWCNT/GONR) was synthesised through a modified oil-bath method similar to that of previous studies.²⁻⁴ MWCNTs (0.05 g) were suspended in $\text{H}_2\text{SO}_4/\text{H}_3\text{PO}_4$ (=9:1, v/v) and stirred for 24 h. KMnO_4 (0.25 g) was then added to the solution before it was placed in an oil bath (66–68 °C) for 8 h. The solution was filtered using a Millipore membrane (0.1 μm pore size) to isolate the product as the residue. The product (MWCNT/GONR) was washed several times with distilled water and freeze-dried for 12 h.

Synthesis of VO_2 and MWCNT/GONR composites.

The VO₂ and MWCNT/GONR composites were synthesised following the same procedures but with the addition of the as-prepared MWCNT/GONR powders. To prepare VO₂/1C, VO₂/2C, and VO₂/3C composite samples, 50, 100, and 150 mg MWCNT/GONR were added into the VO(acac)₂/C₃H₇NO₂S/K₂SO₄ precursor solution, respectively. The precursor solution was then treated by a high-power ultrasonic homogenizer (100-110 W, Qsonica Q700) for 30 min (pulse on 5 s, pulse off 2 s). To avoid heating effect, the precursor solution was immersed in an ice bath during the sonication process. Next, the hydrothermal and heating procedures were the same as the those for preparing the VO₂(P) sample.

Materials characterization.

X-ray diffraction (XRD, Rigaku MiniFlex600 with a Cu K α source), Raman microscopy (Renishaw InVia confocal microscope with 633 nm laser source), thermogravimetric analysis (Perkin Elmer TGA-4000), X-ray photoelectron spectroscopy (XPS, ULVAC-PHI 5000 VersaProbe III equipped with an Al K α radiation), nitrogen adsorption/desorption analysis (Micromeritics ASAP 2020), scanning electron microscopy (SEM, JEOL JSM-7610F Plus equipped with energy-dispersive X-ray spectroscopy, EDS), transmission electron microscopy (TEM, JEOL JEM-2010) were used to analyze the samples.

Electrochemical measurements.

The obtained electroactive material was mixed with Super P and PVDF with a weight ratio of 7:2:1 in NMP solvent. The slurry was then transferred onto carbon paper substrates with the mass loading of ca. 1.2–1.5 mg cm⁻². The electrochemical performance was tested with CR2032 coin-type cells, made of the vanadium oxide electrode, metallic zinc foil, and glass fiber separator. 2 M Zn(TFSI)₂ aqueous solution (100 μ L) was used as the electrolyte unless specifically mentioned. The galvanostatic charge/discharge (GCD) cycles at various current densities (in the range 1–50 A g⁻¹) were measured using LAND CT2001A. The cyclic voltammetric (CV) curves at various scan rates (in the range of 0.2–1.5 mV s⁻¹) were conducted using CH Instruments 6273d. The potential range was controlled as 0.2–1.6 V (vs. Zn²⁺/Zn). For the electronic conductivity tests, the vanadium oxide electrodes were analyzed at room temperature by an alternating current (AC) mode (2 Hz at open circuit potential with the potential amplitude of 10 mV) in an enhanced controlled environment sample holder (CESH-e) using BioLogic SP-300.

Preparation and evaluation of free-standing electrodes.

The procedures for preparing the free-standing electrode at high loading masses were adopted from our previous report.⁵ Typically, 56 mg VO₂/2C powder, 24 mg MWCNTs, and 10 μL Triton X-100 were added into 10 mL deionized water under vigorous stirring for 10 min and ultrasonic treatment for 1 h. Then, the homogeneous suspension was vacuum-filtrated through a PVDF membrane. After thoroughly washing with deionized water and drying at 60 °C for 8 h, the free-standing film was peeled off from the PVDF membrane forming a self-supported electrode. The mass loading of the free-standing electrode is 19.4 mg cm⁻² (based on the mass of VO₂/2C). The electrochemical performance of the high-mass-loading film was evaluated following the same protocols as the electrodes with carbon paper substrates.

2. Supplementary figures

The crystal structures of the VO₂ polymorphs are depicted by the VESTA software. The cif files of the VO₂ polymorphs are from Crystallography Open Database (COD). The COD IDs are 9000071, 1548819, 1530870, 5910277, and 3000344 for VO₂(P), VO₂(R), VO₂(B), VO₂(D), and VO₂(M), respectively. The tunnel size of VO₂(P) is directly adopted from a previous work,⁶ while the values of other VO₂ polymorphs are reported based on the V–O bond lengths from the cif files. Of note, the VO₂/MWCNT/GONR composite samples show mixed phases of VO₂(P), VO₂(A), and VO₂(R). However, the cif file of VO₂(A) is not available in the COD database.

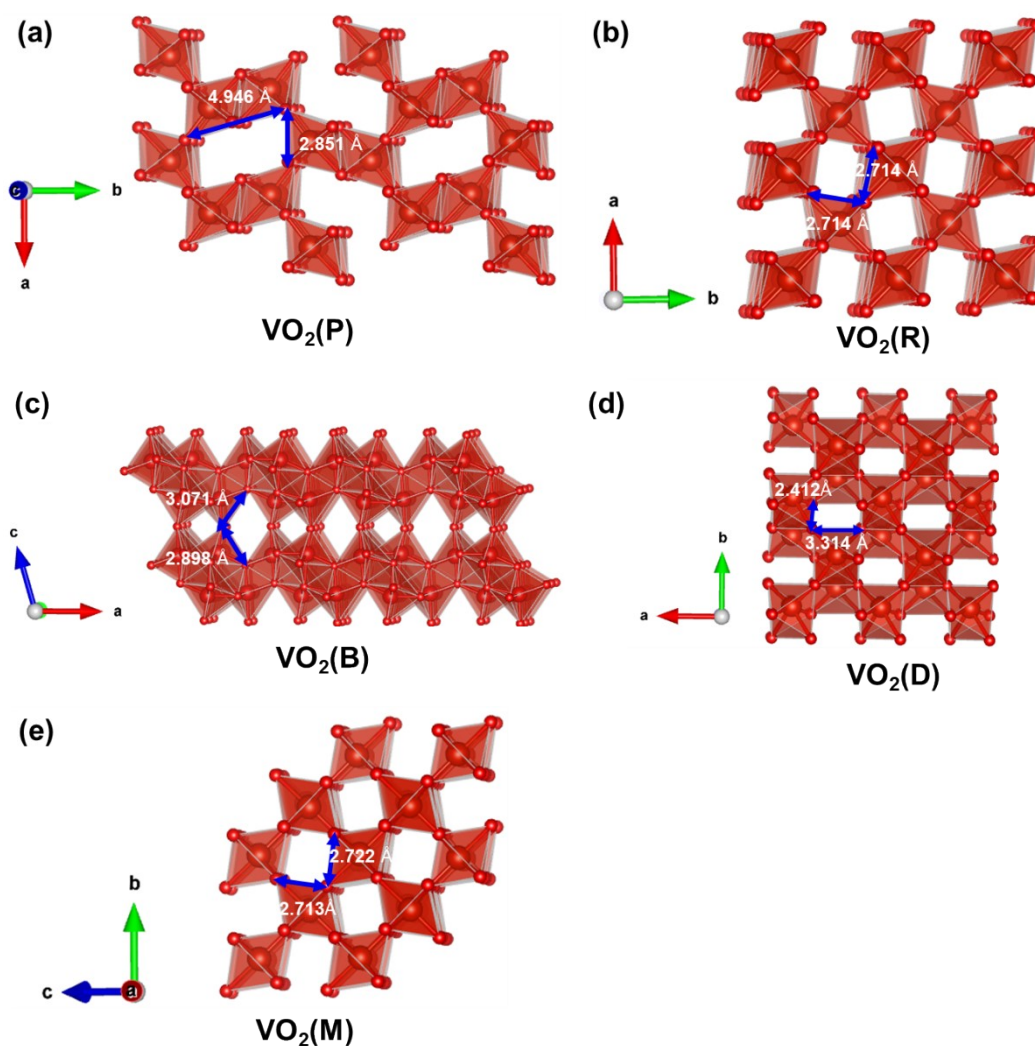


Figure S1. Illustration of the crystal structures of (a) VO₂(P), (b) VO₂(R), (c) VO₂(B), (d) VO₂(D), and (e) VO₂(M).

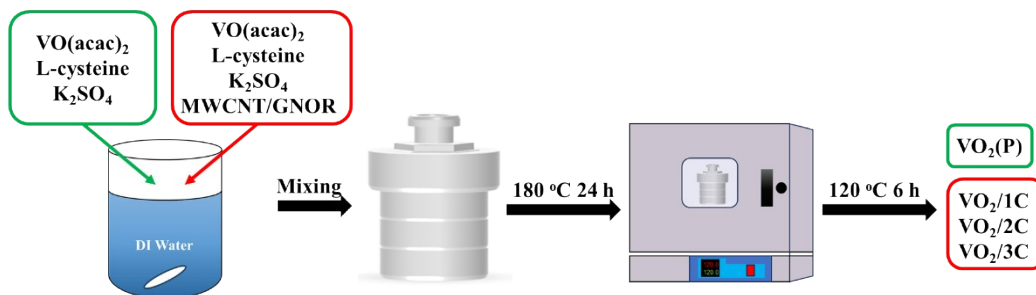


Figure S2. Illustration of the synthetic procedures for $\text{VO}_2(\text{P})$, $\text{VO}_2/1\text{C}$, $\text{VO}_2/2\text{C}$, and $\text{VO}_2/3\text{C}$.

Notably, VO_2 can be oxidised to V_2O_5 at high temperatures in air, leading to mass increase in the weight loss curve. Nitrogen atmosphere was used to avoid this effect. Thus, the detected weight loss better reflects the decomposition of MWCNT/GONR. Notably, the weight loss below 100 °C is attributable to the physisorbed water originating from the ambient environment.⁷ Thus, the weight loss portion below 100 °C is excluded.

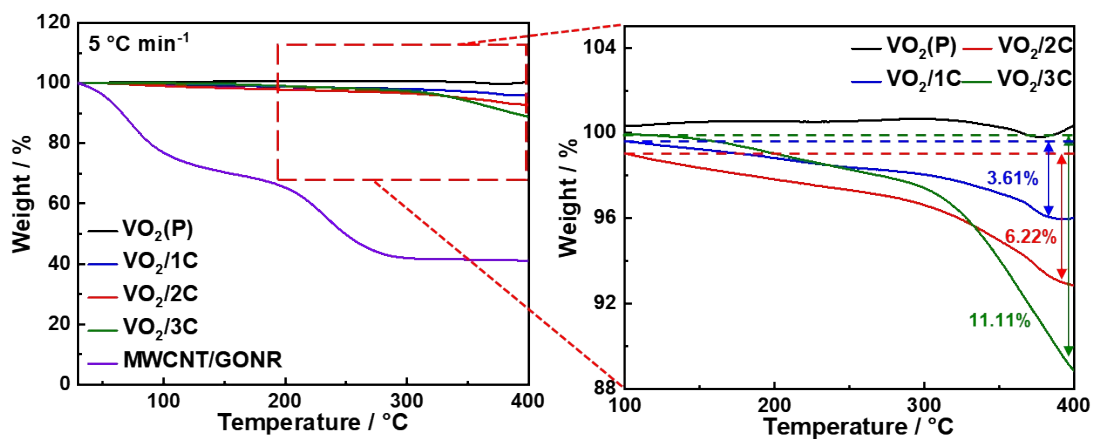


Figure S3. Weight loss curves of $\text{VO}_2(\text{P})$, $\text{VO}_2/1\text{C}$, $\text{VO}_2/2\text{C}$, and $\text{VO}_2/3\text{C}$.

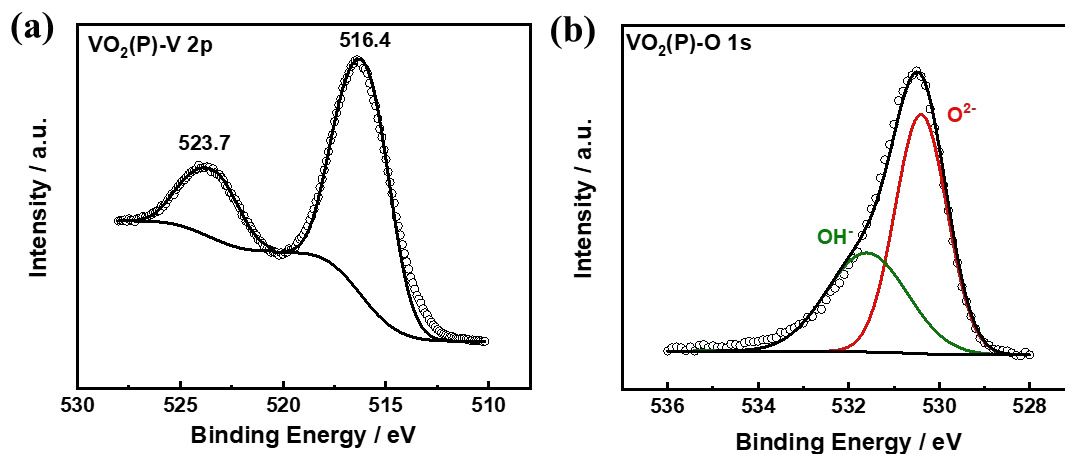


Figure S4. XPS (a) V 2p and (b) O 1s spectra of $\text{VO}_2(\text{P})$.

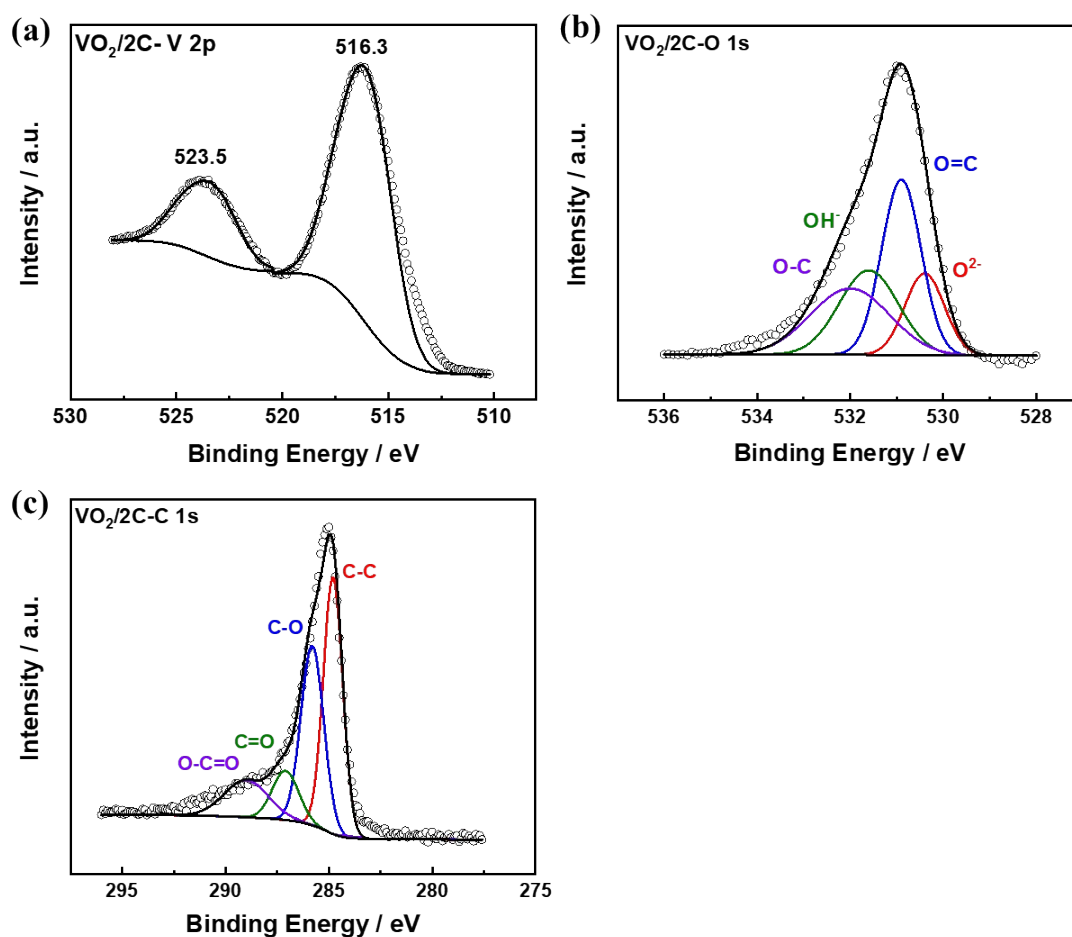


Figure S5. XPS (a) V 2p, (b) O 1s, and (c) C 1s spectra of $\text{VO}_2/2\text{C}$.

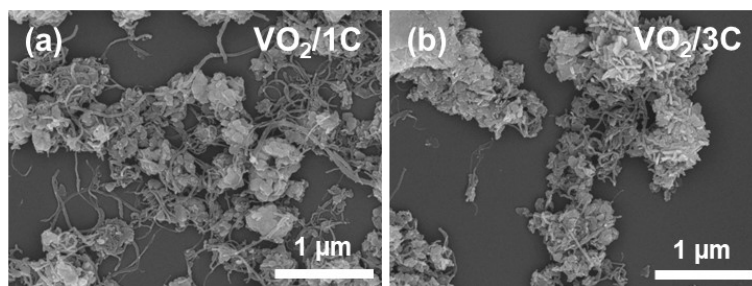


Figure S6. SEM images of (a) VO₂/1C and (b) VO₂/3C.

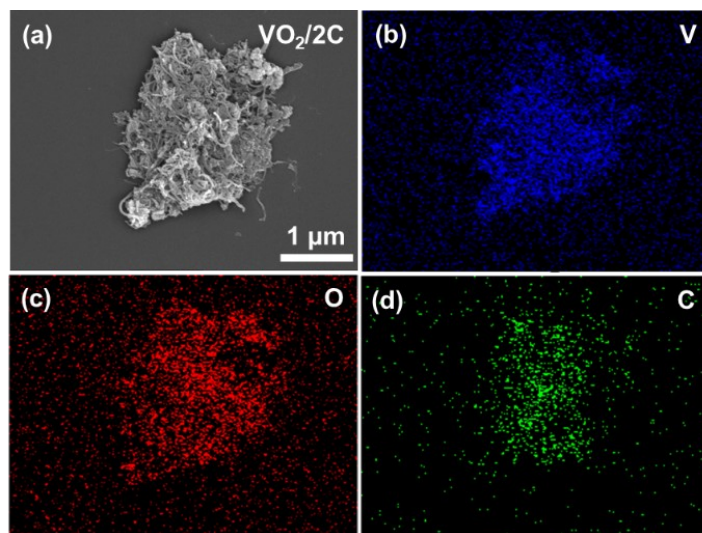


Figure S7. (a) A SEM image and (b-d) the corresponding elemental mapping images of VO₂/2C.

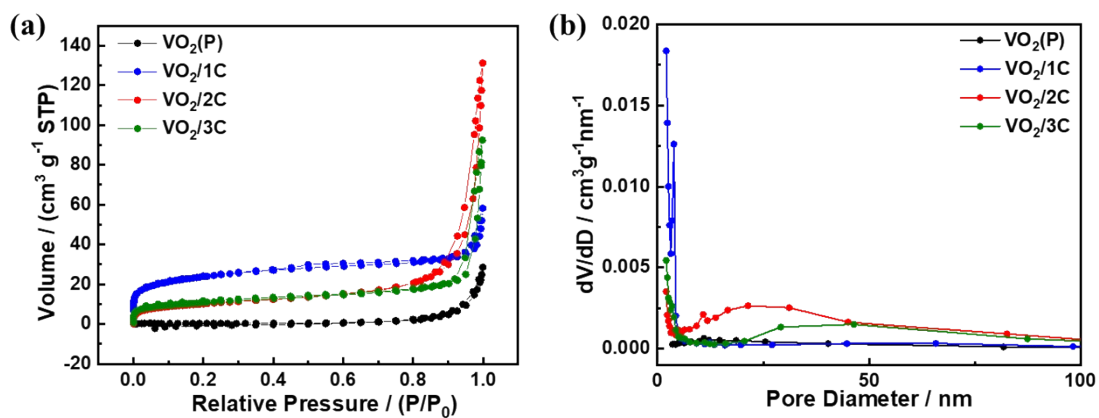


Figure S8. (a) Nitrogen adsorption/desorption isotherms and (b) pore size distribution of VO₂(P), VO₂/1C, VO₂/2C, and VO₂/3C.

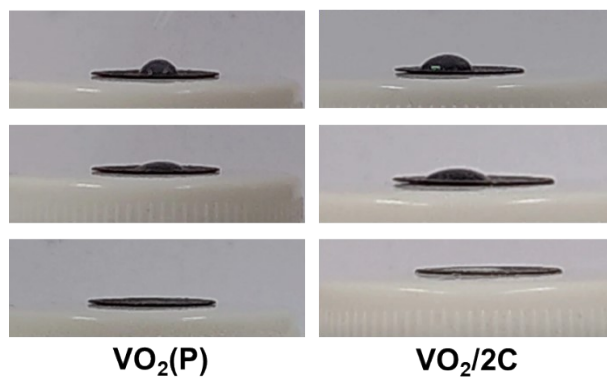


Figure S9. Contact angle images of an electrolyte drop (2 M aqueous $\text{Zn}(\text{TFSI})_2$) on $\text{VO}_2(\text{P})$ and $\text{VO}_2/2\text{C}$ electrodes.

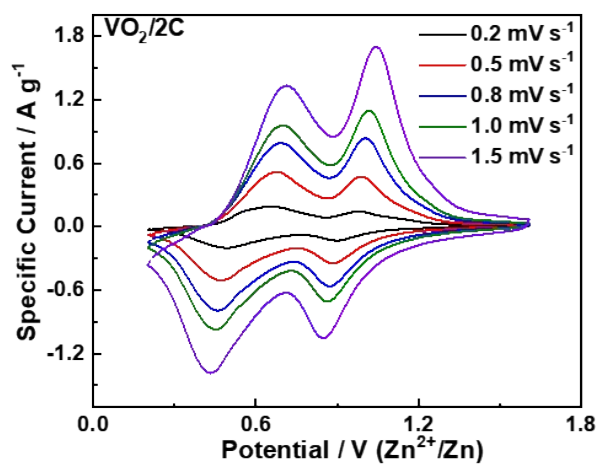


Figure S10. CV curves of $\text{VO}_2/2\text{C}$ at various scan rates.

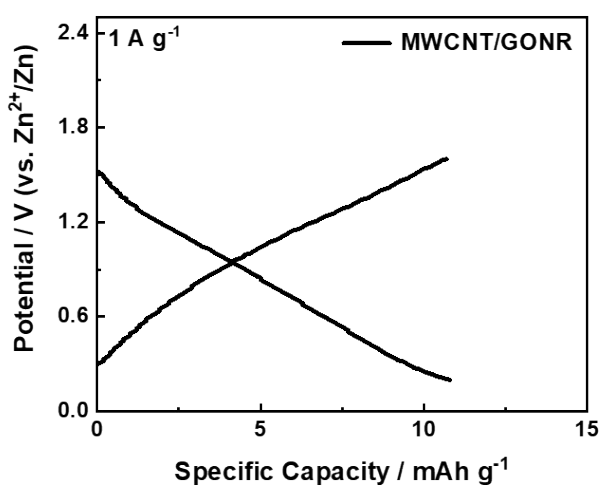


Figure S11. GCD curve of MWCNT/GONR at 1 A g^{-1} .

The current responses in the CV curves can be regarded as the combination of diffusion-controlled (de)intercalation process ($i_2 = k_2v^{1/2}$) and non-diffusion-controlled contribution ($i_1 = k_1v$). As k_1 and k_2 are variable parameters, the (non-)diffusion-controlled contribution ratios can be determined by b -value fitting analysis (Fig. S12c).^{8,9} The fitting results are summarized in Fig. S12d.

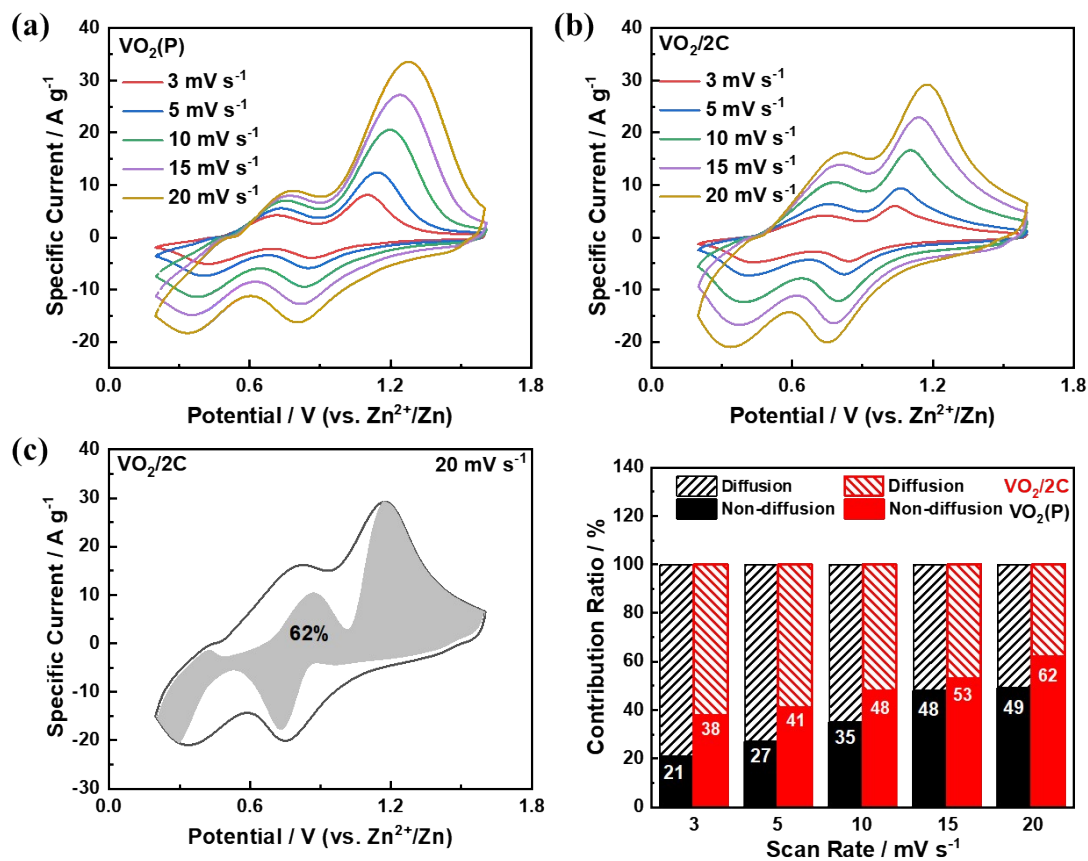


Figure S12. CV curves of (a) VO₂(P) and (b) VO₂/2C; (c) evaluation of non-diffusion-controlled contribution of VO₂/2C at 20 mV s⁻¹; (d) (non-)diffusion-controlled contribution ratios of VO₂(P) and (b) VO₂/2C.

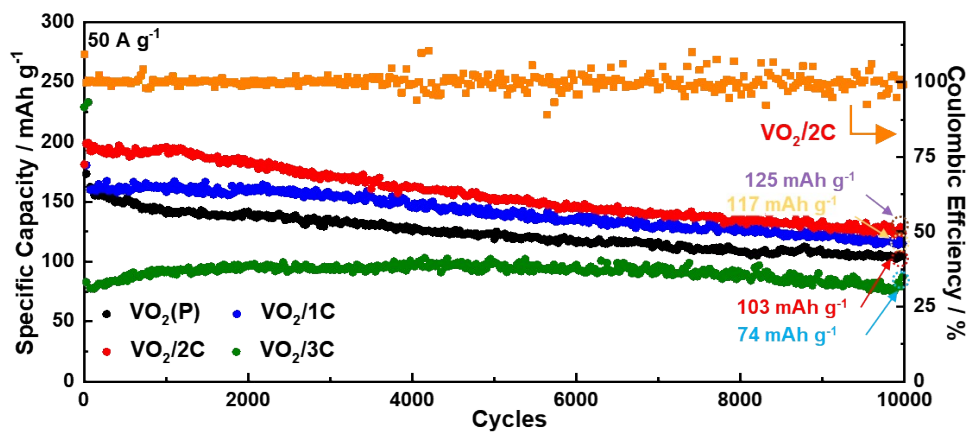


Figure S13. Cycle performance of VO₂(P), VO₂/1C, VO₂/2C, and VO₂/3C at 50 A g⁻¹.

3. Supplementary Tables

Table S1. The pore volume and specific surface area values of the samples from nitrogen adsorption/desorption analysis (Fig.S8).

Sample	Pore volume (cm ³ g ⁻¹)	Specific surface area (m ² g ⁻¹)
VO ₂ (P)	0.044	0.9
VO ₂ /1C	0.090	81.1
VO ₂ /2C	0.203	35.6
VO ₂ /3C	0.143	34.4

Table S2. Comparisons of battery performance of VO₂ polymorphs and their composite positive electrode materials used in AZIBs.

Positive electrode material	Electrolyte	Discharge capacity (mAh g ⁻¹ / A g ⁻¹)	Specific capacity (mAh g ⁻¹)/ cycles/ current density (A g ⁻¹)
VO₂(P)/GONR this work	2 M Zn(TFSI)₂	428 at 1.0 A g⁻¹ 349 at 10 A g⁻¹ 208 at 50 A g⁻¹	294 / 1000 / 10 181 / 10000 / 50
H-doped VO ₂ (B) ¹⁰	3 M Zn(CF ₃ SO ₃) ₂	~475 at 1.0 A g ⁻¹ ~150 at 10 A g ⁻¹	~85/ 22000 / 10
VO ₂ (D) ¹¹	3 M ZnSO ₄	382 at 1.0 A g ⁻¹ 262 at 10 A g ⁻¹	89 / 30000 / 10
VO ₂ (R) ¹²	1 M ZnSO ₄ (70 °C)	~175 at 1 A g ⁻¹ 76 at 10 A g ⁻¹	122 / 170 / 2
VO ₂ (B)/rGO ¹³	3 M Zn(CF ₃ SO ₃) ₂	384 at 1 A g ⁻¹ 292 at 10 A g ⁻¹	283 / 1000 / 5
VO ₂ (B)/rGO ¹⁴	3 M Zn(CF ₃ SO ₃) ₂	~237 at 1 A g ⁻¹ 194 at 8 A g ⁻¹	240 / 1000 / 4
VO ₂ (B)/CQDs ¹⁵	3 M ZnSO ₄	381 at 1 A g ⁻¹ 309 at 8 A g ⁻¹	229 / 2000 / 4
holey C@VO ₂ (B) ¹⁶	3 M Zn(CF ₃ SO ₃) ₂	291 at 1 A g ⁻¹ 208 at 5 A g ⁻¹	280 / 600 / 5
VO ₂ (A)@NC ¹⁷	3 M Zn(CF ₃ SO ₃) ₂	450 at 1 A g ⁻¹ 363 at 8 A g ⁻¹	269 / 2500 / 10

Table S3. Comparisons of battery performance of ultrahigh rate positive electrode materials used in AZIBs.

Positive electrode material	Electrolyte	Voltage window (V)	Discharge capacity (mAh g ⁻¹ / A g ⁻¹)	Specific capacity (mAh g ⁻¹)/ cycles/ current density (A g ⁻¹)
VO₂(P)/GONR this work	2 M Zn(TFSI)₂	0.2~1.6	428 at 1 A g⁻¹ 349 at 10 A g⁻¹ 208 at 50 A g⁻¹	294 / 1000 / 10 181 / 10000 / 50
VO ₂ (M)/CNT ¹⁸	2 M ZnSO ₄	0.3~1.5	240 at 10A g ⁻¹ 195 at 40 A g ⁻¹	~195 / 5000 / 20
V ₂ O ₃ /CNT ¹⁹	2 M Zn(CF ₃ SO ₃) ₂	0.2~1.6	300 at 10 A g ⁻¹ 211 at 50 A g ⁻¹	237 / 5000 / 10
heterostructured VO ₂ (B)-rGO (VO _x -rGO) ²⁰	3 M Zn(CF ₃ SO ₃) ₂	0.3~1.5	~350 at 10 A g ⁻¹ ~240 at 50 A g ⁻¹ 174 at 100 A g ⁻¹	~280 / 1000 / 20
VN _{0.9} O _{0.15} ²¹	3 M Zn(CF ₃ SO ₃) ₂	0.2~1.8	~215 at 8.5 A g ⁻¹ ~155 at 51.2 A g ⁻¹ 124 at 102.4 A g ⁻¹	139 / 1500 / 4.3
Na _{0.12} Zn _{0.25} V ₂ O ₅ ·2.5H ₂ O (NZVO) ²²	3 M Zn (CF ₃ SO ₃) ₂	0.3~1.6	357 at 10 A g ⁻¹ 268 at 50 A g ⁻¹ 92 at 400 A g ⁻¹	~95 / 140000 / 200
Amorphous VEG-VO _x	3 M Zn (CF ₃ SO ₃) ₂	0.2~1.7	~363 at 10 A g ⁻¹	~138 / 17000 / 100

(AOH-VO) ²³			~244 at 50 A g ⁻¹ 121 at 100 A g ⁻¹	
VO ₂ (B) nanofibers ²⁴	3 M Zn (CF ₃ SO ₃) ₂	0.3~1.5	232 at 8.5 A g ⁻¹ 171 at 51.2 A g ⁻¹	250 / 300 / 085
Protonated δ-MnO ₂ ²⁵	2 M ZnSO ₄ + 0.2 M MnSO ₄	1.0~1.9	~145 at 10 A g ⁻¹ 83 at 50 A g ⁻¹	95 / 1100 / 10
Zn-I ₂ ²⁶	2 M ZnSO ₄ + 0.5 M TAH	0.6~1.9	~440 at 2 A g ⁻¹ ~225 at 40 A g ⁻¹	~4365 / 5000 / 2
Mn-Fe PBA ²⁷	1 M ZnSO ₄	0~2.2	157 at 1 A g ⁻¹ 47 at 10 A g ⁻¹	46 / 3000 / 5

TAH and PBA stand for trimethylamine hydrochloride and Prussian blue analogue, respectively.

4. References

1. Y. Xu, L. Zheng and Y. Xie, *Dalton Trans.*, 2010, **39**, 10729-10738.
2. D. V. Kosynkin, A. L. Higginbotham, A. Sinitskii, J. R. Lomeda, A. Dimiev, B. K. Price and J. M. Tour, *Nature*, 2009, **458**, 872-876.
3. C. L. Sun, C. T. Chang, H. H. Lee, J. Zhou, J. Wnag, T. K. Sham and W. F. Pong, *ACS Nano*, 2011, **5**, 7788-7795.
4. W. H. Lin, S. F. Liu, S. Gull, T. C. Su, K. J. Tsai, C. H. Kuo, C. C. Lin, C. C. Wang, M. H. Lin, C. L. Sun and H. Y. Chen, *J. Power Sources*, 2022, **541**, 231627.
5. T. H. Wu, T. K. Li and L. J. Guo, *J. Power Sources*, 2024, **623**, 235503.
6. C. Wu, Z. Hu, W. Wang, M. Zhang, J. Yang and Y. Xie, *Chem. Commun.*, 2008, DOI: 10.1039/b806009f, 3891-3893.
7. H. Yu, M. Aakyiir, S. Xu, J. D. Whittle, D. Losic and J. Ma, *Mater. Today Energy*, 2021, **21**, 100757.
8. W. Lv, J. Meng, X. Li, C. Xu, W. Yang, S. Duan, Y. Li, X. Ju, R. Yuan, Y. Tian, M. Wang, X. Lyu, P. Pan, X. Ma, Y. Cong and Y. Wu, *Energy Storage Mater.*, 2023, **54**, 784-793.
9. W. Lv, Z. Shen, X. Li, J. Meng, W. Yang, F. Ding, X. Ju, F. Ye, Y. Li, X. Lyu, M. Wang, Y. Tian and C. Xu, *Nano-Micro Lett.*, 2024, **16**, 109.
10. K. Guan, K. Duan, G. Yang, L. Tao, H. Zhang, H. Wan, R. Yang, J. Zhang, H. Wang and H. Wang, *Mater. Today Adv.*, 2022, **14**, 100230.
11. L. Chen, Z. Yang and Y. Huang, *Nanoscale*, 2019, **11**, 13032-13039.
12. B. Aydogdu, S. Aydin, S. P. Sasikala, H. E. Unalan, S. O. Kim and R. Yuksel, *J. Energy Storage*, 2024, **86**, 111264.
13. F. Cui, J. Zhao, D. Zhang, Y. Fang, F. Hu and K. Zhu, *Chem. Eng. J.*, 2020, **390**, 124118.
14. X. Dai, F. Wan, L. Zhang, H. Cao and Z. Niu, *Energy Storage Mater.*, 2019, **17**, 143-150.
15. T. H. Wu, J. A. Chen, J. H. Su and Y. H. Ting, *J. Energy Storage*, 2023, **74**, 109340.
16. M. Yang, D. Ma, H. Mi, X. Yang, Y. Wang, L. Sun and P. Zhang, *J. Mater. Chem. A*, 2021, **9**, 8792-8804.
17. T.-T. Lv, X. Luo, G.-Q. Yuan, S.-Y. Yang and H. Pang, *Chem. Eng. J.*, 2022, **428**, 131211.
18. L. Zhang, L. Miao, B. Zhang, J. Wang, J. Liu, Q. Tan, H. Wan and J. Jiang, *J. Mater. Chem. A*, 2020, **8**, 1731-1740.
19. J. S. Park, S. Yang and Y. C. Kang, *Small Methods*, 2021, **5**, e2100578.
20. Y. Dai, X. Liao, R. Yu, J. Li, J. Li, S. Tan, P. He, Q. An, Q. Wei, L. Chen, X.

- Hong, K. Zhao, Y. Ren, J. Wu, Y. Zhao and L. Mai, *Adv. Mater.*, 2021, **33**, 2100359.
21. J. Ding, Z. Du, B. Li, L. Wang, S. Wang, Y. Gong and S. Yang, *Adv. Mater.*, 2019, **31**, 1904369.
 22. L. Wang, J. Yan, Y. Hong, Z. Yu, J. Chen and J. Zheng, *Sci. Adv.*, 2023, **9**, eadf4589.
 23. M. Liu, X. Li, M. Cui, F. Chen, J. Li, W. Shi, Y. Liu, X. Li, Y. Wang, W. Zhang, C. Shao and Y. Liu, *Nat. Commun.*, 2024, **15**, 10769.
 24. J. Ding, Z. Du, L. Gu, B. Li, L. Wang, S. Wang, Y. Gong and S. Yang, *Adv. Mater.*, 2018, **30**, 1800762.
 25. Y. Zuo, P. Liu, L. Ling, M. Tian, Z. Wang, H. Tian, T. Meng, X. Sun and S. Cai, *ACS Appl. Mater. Interfaces*, 2022, **14**, 26653-26661.
 26. M. Wang, Y. Meng, M. Sajid, Z. Xie, P. Tong, Z. Ma, K. Zhang, D. Shen, R. Luo, L. Song, L. Wu, X. Zheng, X. Li and W. Chen, *Angew. Chem. Int. Ed.*, 2024, **63**, e202404784.
 27. H. Fu, X. Wang, L. Ye, Z. Wu, J. Yang, M. Shi and E. H. Ang, *Chem. Eng. J.*, 2025, **506**, 160308.